crystals

MDPI

Article

Inclusion Complexes of Naringenin in Dimethylated and Permethylated β-Cyclodextrins: Crystal Structures and Molecular Dynamics Studies

Andreas Papaioannou, Elias Christoforides and Kostas Bethanis *

Physics Laboratory, Department of Biotechnology, School of Applied Biology and Biotechnology Agricultural University of Athens, Iera Odos 75, 11855 Athens, Greece; apapaioannou@efet.gr (A.P.); el_chr@aua.gr (E.C.)
* Correspondence: kbeth@aua.gr; Tel.: +30-210-529-4211

Received: 25 November 2019; Accepted: 20 December 2019; Published: 24 December 2019

Abstract: The crystal structures of the inclusion complexes of naringenin in dimethylated and permethylated β-cyclodextrin (DM-β-CD and TM-β-CD) were determined and extensively analyzed. Naringenin is found with its 4-hydroxyphenyl residue fully immersed in the DM-β-CD cavity and its chromone group protruding from the narrow rim of the open-cone shaped host. The naringenin/DM-β-CD complex units are packed in a 'herring bone' fashion. In the case of naringenin/TM-β-CD, the complex units are arranged in a cage-type mode, the guest naringenin is partially encapsulated in the cavity of the closed-cone shaped host, with its chromone group laying equatorially and its 4-hydroxyphenyl protruding extensively from the wide rim of the host. Furthermore, the crystallographically-determined coordinates of both complexes were employed for Molecular Dynaimics simulations in explicit water solvent and in the absence of crystal contacts. The trajectories showed that naringenin rapidly penetrates the open narrow rim of DM-β-CD but not the closed narrow rim of TM-β-CD. Thus, in the latter case, the chromone group of naringenin is accommodated shallowly in the wide rim of the host, tethered via hydrogen bonds to the secondary methoxy groups of the host. Finally, a significantly higher binding affinity for naringenin in DM-β-CD than TM-β-CD was estimated by Molecular Mechanics/Generalized Born Surface Area calculations.

Keywords: naringenin; heptakis(2,6-di-*O*-methyl)-β-cyclodextrin; heptakis(2,3,6-tri-*O*-methyl)-β -cyclodextrin; crystal structures; molecular dynamics

1. Introduction

Naringenin ((±)-2,3-dihydro-5,7-dihydroxy-2-(4-hydroxyphenyl)-4*H*-1-benzopyran-4-one) or (5,7-dihydroxy-2-(4-hydroxyphenyl)chroman-4-one) (Figure 1a) is the aglycone part of naringin, which is a flavonoid glycoside mainly found in citrus fruits [1]. Its structure comprises a chromone group (rings A and C) and a 4-hydroxyphenyl residue (ring B). There is an increased interest in naringenin in food and drug industry, which is attributed to its anti-inflammatory, anticancer, antiatherogenic, antitumor, anti-estrogenic, and antioxidant properties [2–5]. Its ability to reduce or block harmful metabolic procedures [6], like plasma cholesterol levels or the activity of the hepatitis C virus, has also been demonstrated.

Despite the above benefits, naringenin's low half-life, water solubility, and stability result in limited bioavailability and potential uses. One way to overcome these problems is the inclusion of naringenin in cyclodextrins (CDs) [7,8]. β-Cyclodextrin (β-CD) is a well-known, hollow, truncated, cone shaped oligosaccharide consisting of seven α-(1−4)-linked D-glucose residues. The shape and size of the hydrophobic β-CD cavity enables the formation of inclusion complexes with a variety of suitable guest molecules of food, agricultural, and pharmaceutical interest [9–12]. The low

β-CD solubility is significantly increased by the methylation of two or three hydroxyl groups of each glucopyranose unit. The methylated *β*-CD derivatives—2,6-di-O-methyl-*β*-CD (DM-*β*-CD) and 2,3,6-tri-O-methyl-*β*-Cyclodextrin (TM-*β*-CD) (Figure 1b)—have, in addition, an increased inclusion capacity [13].

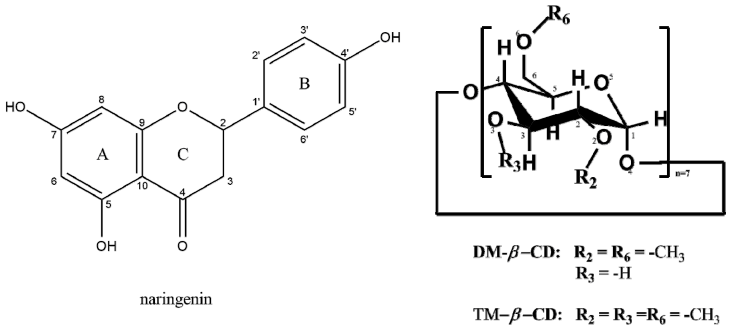

Figure 1. Schemes of (**a**) naringenin and (**b**) heptakis (2,6-di-*O*-methyl)-*β*-cyclodextrin (DM-*β*-CD) and heptakis (2,3,6-tri-*O*-methyl)-*β*-cyclodextrin (TM-*β*-CD).

The inclusion of naringenin in native and modified cyclodextrins has been extensively characterized by UV-Vis, FTIR [14,15], NMR, XRD, DSC/TGA, and SEM [16,17] techniques. Moreover, computational studies of molecular docking and subsequent MD simulations have been performed [7,18]. However, no crystal structure of naringenin inclusion complexes in CDs have been reported so far. In this work, the crystal structures of the inclusion complexes of naringenin in DM-*β*-CD and TM-*β*-CD were determined by X-ray crystallography. The analysis of the crystal structures offers unique information about the relative atomic positions of the guest and host molecules, revealing the inclusion geometry, the intra- and inter-molecular interactions, and the molecular arrangement of the complex units in the crystalline state. Furthermore, the atomic coordinates determined by X-ray crystallography were employed for molecular dynamics (MD) simulations of these inclusion complexes in explicit water solvent at 300 K. The simulations were analyzed with the aim to (a) gain insight into the dynamic behavior and the stability of the inclusion complexes in aqueous ambient and in the absence of crystal contacts, (b) monitor the main host-guest interactions that are responsible for the binding modes, and (c) observe any interconversion of inclusion modes in solution. Finally, the stability of the examined inclusion complexes was assessed by the molecular mechanics/generalized Born surface area (MM/GBSA) method, calculating the binding affinity of the complexes.

2. Results

2.1. Crystal Structures Description

2.1.1. Naringenin/DM-β-CD Inclusion Complex

The naringenin/DM-*β*-CD inclusion complex crystallizes in the $P2_12_12_1$ space group, its asymmetric unit containing one DM-*β*-CD, one naringenin, and 4.6 water molecules disordered over 9 sites. The 4-hydroxyphenyl residue (ring B in Figure 1a) of naringenin is fully immersed in the host cavity, forming an angle of 69.31° with the mean plane of the glycosidic atoms O4(*n*) (*n* = 1–7) of the host. The hydroxyl group of this ring points towards the wide rim of the host, being at a distance of 1.514 Å 'below' the O4(n) mean plane of the host (Figure 2a) and forming a hydrogen bond with the etheric O5(4) atom of the adjacent host and CH … O bonds with the primary methoxy groups of the adjacent host. Ring B is further stabilized by a CH/π interaction between its π system and the C5(5)−H5(5) inner hydrogen of the host's cavity (Supplementary Table S1(a1,2). The chromone ring system of naringenin (5,7-dihydroxychromone residue; rings A and C in Figure 1a) forms an angle of 77.261(4)°

with the phenyl ring B and protrudes extensively from the primary rim of the host. The ring C, which is closer to the primary rim of the host, forms CH ... O bonds with the primary methoxy groups of the host (Table S1(a1)). The ring A is located outside the host cavity in the interspace of neighboring complex units. Its hydroxyl at position 7 (Figure 1a) is hydrogen-bonded with a water molecule (fully occupied site Ow1) that bridges the adjacent complex units. Both hydroxyls of ring A (at positions 5 and 7) form CH ... O bonds with the methoxy groups of neighboring hosts (Table S1(a1)). In addition, the chromone group of the guest molecule is further stabilized by several CH/π interactions between the π-system of ring A and the methoxy groups of neighboring hosts (Table S1(a2)). It should be noted that the inclusion mode observed in the crystal structure of naringenin/DM-β-CD, with the guest molecule entering from the primary rim of the host, is opposite to that previously predicted by molecular docking studies [18] or 2D-NMR (ROESY) spectrum analysis from NMR experiments carried out in D_2O [14], which presented the guest molecule inserting from the secondary rim of the host and its ring B accommodated in the cavity of the host with its hydroxyl pointing towards the primary rim and its chromone group protruding from the wide rim of the host.

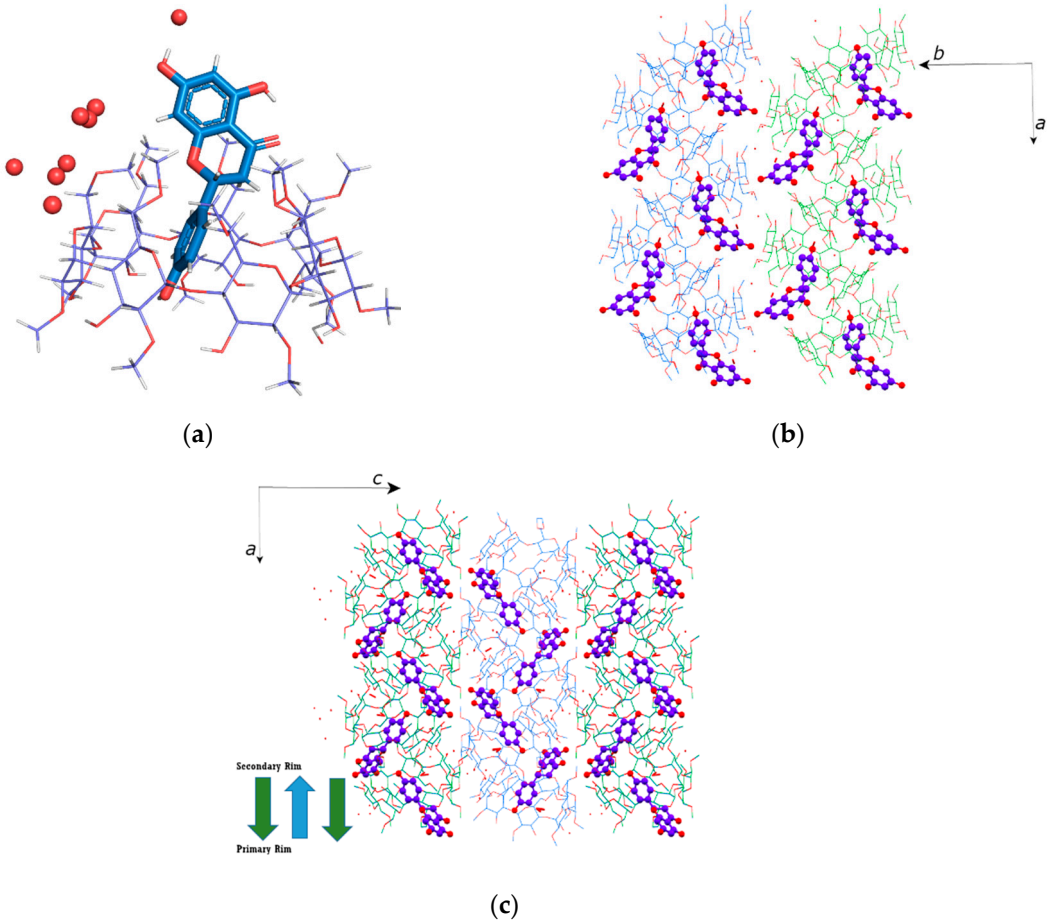

Figure 2. (**a**) The asymmetric unit of the naringenin/DM-β-CD inclusion complex crystal structure. One guest molecule is partially encapsulated inside the host's cavity with its 4-hydroxyphenyl residue (ring B) entering from its primary rim; (**b**) complex units are packed in a 'herring bone' fashion along the *a*-axis. These columns are deployed parallel along the *b*-axis (*ab*-plane projection); and **(c)** anti-parallel along the *c*-axis (*ac*-plane projection).

The geometric features of the host, summarized in Table S2(a1), indicate, in general, a round conformation of the macrocycle of DM-β-CD, having the usual torus-like shape. This conformation is mainly due to the interglucose hydrogen bonds O3(n)-H···O2(n+1) [19], formed between the adjacent glucopyranose units of DM-β-CD. An exception in the formation of these hydrogen bonds occurs

between the second (G2) and the third (G3) glucopyranose as the distance between O3(2) and O2(3) atoms is 3.324(3) Å. This results in a slight deviation from the ideal sevenfold symmetry of the macrocycle of the host (D_k: distances between O4n atoms and their centroid, range from 4.9230(2) to 5.3577(3) Å; Φn: O4n−1 ... O4n ... O4n+1 angles from 115.895(11)° to 140.256(6)°). It should be noted that an extra partial methylation (with site occupation factor, s.o.f = 0.7) has been observed in the O3(2)-H of G2 of DM-β-CD as the commercial product agent used had over-methylated homolog impurities. In the absence of this methylation, the O3(2)H hydroxyl (s.o.f = 0.3) is hydrogen-bonded to the OW36 site that is also 30% occupied by the oxygen atom of a water molecule, which, in turn, is hydrogen-bonded to another water molecule (OW7; s.o.f. = 0.3) (Table S1(a3)). The tilt angles τ, indicating the inward or outward inclination of the primary methoxy groups of the host cavity, range from 2.6755(2)° to 24.7479(9)°. The high values of τ angles, which are observed for the G1 and G2 and their facing G5 and G6 glucopyranoses, indicate a widening of the secondary rim toward the direction determined by these facing residues that is justified by the arrangement of the adjacent complex unit, as described below.

Naringenin, inserting from the narrow side of the host, is partially encapsulated in the DM-β-CD cavity while the interior space of the wide side of the host is essentially empty. This allows complex units to develop the self-inclusion tendency of the DM-β-CD hosts [20] and, thus, arrange themselves accordingly in the crystal structure. In particular, adjacent complex units are packed in a 'herring bone' mode parallel to the *a*-axis, inclined at 26.56° against the *bc* plane. The mean O4(n) planes of the adjacent hosts in this 'herring bone', form angles of 53.12° between each other. The primary methoxy of the G4 glucopyranose of the host 'below' intrudes deeply into the wide rim of the cavity of the host 'above', its O5(4) atom being hydrogen-bonded with the hydroxyl of the ring B of the encapsulated guest molecule (Table S1(a1) and Figure 2b). The methoxy groups of the neighboring G4 glucopyranoses (G3 and G5) are also located in the wide rim of the host above. The columns of this 'herring bone' arrangement are deployed parallel to each other along the *b*-axis and are antiparallel, shifted by 5.581(3) Å along the *c*-axis (Figure 2c), and interconnected via hydrogen bonds with bridge water molecules (Table S1(a3)). DM-β-CD inclusion complexes with similar packing arrangement also have a similar degree of hydration (about 4.5 water molecules per asymmetric unit) [21]. The 'herring bone' fashion arrangement has been observed in the crystal structure of anhydrous DM-β-CD [22], where a O6-C8 methoxy group of one molecule is inserted into the next molecule by self-inclusion. Anhydrous DM-β-CD also crystallizes in $P2_12_12_1$ with cell dimensions close to those of the naringenin/DM-β-CD crystal structure and, similarly, a neighboring O6-C8 methoxy group inserts deeply into the DM-β-CD cavity, filling the space and closing the wide rim of DM-β-CD.

A thorough search in the Cambridge Structural Database (CSD), using cell check v 1.0, resulted in two entries for crystal structures of native β-CD inclusion complexes that share similar cell dimensions (94.5% and 91.4% cell match, respectively) and the same space group. However, both of them—monomer (2-(2,6-dichloro-3-methylphenylamino)benzoate/β-CD (CCDC code: MANNOE) and monomer (3-(10,11-dihydro-5H-dibenzo[*a*,*d*][7]annulen-5-ylidene)-N,N-dimethylpropan-1-amine/β-CD (CCDC code: MEJHAN)—form channels along the *b*-axis.

2.1.2. Naringenin/TM-β-CD Inclusion Complex

The naringenin/TM-β-CD inclusion complex crystallizes anhydrous in the $P2_1$ space group. The asymmetric unit consists of one TM-β-CD molecule hosting one naringenin molecule, which is found disordered over two close sites (site A and site B) of equal occupancy (s.o.f. = 0.5). The inclusion mode is similar for both occupied sites: the chromone group of the guest molecule lays equatorially in the wide rim of the host, with its plane forming an angle of about 80.4° (site A) or 88.3° (site B) with the O4(n) mean plane of the host, whereas the 4-hydroxyphenyl residue (ring B) of the guest molecule protrudes from the wide rim of the host in the interspace of neighboring complex units (Figure 3a). The main difference between the two occupied sites of the guest molecule is that the ring B is found slightly shifted by 1.051(2) Å (distance between the centroid of ring B in site A and B) and rotated about

the C1′–C2 axis of the molecule, forming an angle of 83.65(2)° and 69.64(3)° with the mean plane of the chromone ring system for the site A and B, respectively. For both sites, the hydroxyl of the ring B is hydrogen-bonded with the O3(6) atom of a secondary methoxy group of an adjacent (1+x, y, −1+z) host (Table S1(b1)). In the case of site A, the O4′ atom of its hydroxyl also participates in CH ... O bonds with the methyls of primary and secondary methoxy groups of three adjacent hosts. In the case of site B, the ring B is further stabilized by CH ... O bonds between its C2′-H2′ and the O2(1) of the host and its C3′-H3′ with the O6(6) (x, 1+y, z) of an adjacent host (Table S1(b1)). Moreover, CH/π interactions are observed between the π-system of the ring B of the guest molecule and methyls of the primary methoxy groups of adjacent hosts for both sites (Table S1(b2)). The ring system of the chromone group of the guest molecule (rings A and C) is stabilized by various hydrogen bonds, CH ... O bonds, and CH/π interactions with its encapsulating host and the hosts of adjacent complex units. In particular, a hydrogen bond is observed for both occupied A and B sites between the hydroxyl at position 7 of the ring A and the oxygen of a secondary methoxy group of a neighboring guest molecule (O7-H7 ... O3(4) (−x, $\frac{1}{2}$+y, 1−z); Table S1(b1)). In the case of the occupied site B, an additional hydrogen bond is observed between the second hydroxyl of the ring A (at position 5) and the oxygen atom of a primary methoxy group of the encapsulating host (O5-H5 ... O6(7); Table S1(b1)). Ring A and ring C of both occupied sites also participate in numerous CH ... O bonds with the methoxy groups of the encapsulating host and the adjacent hosts. Furthermore, CH/π interactions are observed between the π-system of the ring A and methyl groups of the hosts. All these interactions are given analytically in the supplementary Table S1(b1,2)

The geometrical features given in Table S2(a2) describe the conformation of TM-*β*-CD. As it is indicated by the values in this table, TM-*β*-CD is severely distorted, lacking the intramolecular interglucose hydrogen bonds responsible for the round conformation of the host molecule, observed in the case of the naringenin inclusion complex in DM-*β*-CD. The deviation in the glycosidic O4(n) atoms from their mean plane, ranges from −0.805(10) to 0.625(8) Å. The distances between the O4(n) atoms and their centroid also vary significantly (from 4.398(6) to 5.310(8) Å), indicating a distorted macrocycle that has the shape of an elliptical heptagon. The long axis of this elliptical shape coincides with the orientation of the equatorially-accommodated chromone group of the guest molecule in the wide rim of the host, highlighting the induced-fit mechanism of complexation. The tilt angles of the permethylated glucopyranose units of the host (τ**:** tilt angles between the optimum O4(n) mean plane and the mean plane of the O4(n−1), C1(n), C4(n), and O4(n) atoms) span a wide range from −17.28(16)° to 47.61(15)°, indicating a closed primary rim and a broad secondary rim for the host molecule (Table S2(a2)). In particular, five methyl-glucose residues with positive tilt angles incline towards the approximate sevenfold molecular axis, whereas two residues (G1 and G5) have negative tilt angles. The high τ values of G3, G6, and especially G7, indicate the formation of the characteristic 'lid' in the primary region of the host molecule commonly observed in TM-*β*-CD inclusion complexes. Thus, the host has the shape of a closed cone that the guest molecule cannot penetrate and, therefore, it remains shallowly accommodated in the secondary rim of the host. The secondary methoxy groups of the G6 and G7 units are significantly lifted above the mean plane of the rest of the secondary methoxy groups, leaving a space suitable for the protrusion of the 4-hydroxyphenyl residue of the guest molecule (ring B) from the wide rim of the host molecule. The primary methoxy groups of the host molecule adopt the usual cyclodextrin gauche-gauche and gauche-trans conformations, except for a partially occupied site with low occupancy (0.2) that has the rare trans-gauche conformation, as it is indicated by the values of the O5n-C5n-C6n-O6n torsion angles (*t*).

In the absence of bridge water molecules, the complex units stack in a head-to-tail mode along the two-fold screw *b*-axis with their mean O4 planes slanted at 33.65(2)° against the *ac* plane (Figure 3b). The complex units of these columns are interconnected via numerous host-adjacent guest molecule and host-adjacent host molecule CH ... O and CH/π interactions that have been described above (Table S1(b1,2)). The columns are deployed along the crystallographic *a*- and *c*-axes. However, the complex units of the columns deployed along the *a*-axis have opposite inclinations to those of the columns

deployed along the *c*-axis. Thus, each column is surrounded by neighboring ones with complex units of opposite inclination (Figure 3b). In this arrangement, each complex unit is tightly packed in a cage-type mode, its wide rim blocked by the primary methoxy groups of the adjacent host molecule of the same column and the secondary methoxy groups of the host molecules of the neighboring columns that form H-bonds with the hydroxyls of the A and B rings of the encapsulated guest molecule (Figure 3c). Although similar cage-type packing has been previously reported for TM-*β*-CD inclusion [23], this is a unique crystal packing as no isostructural entries were found in CSD by thoroughly searching similar cell dimensions and same space group.

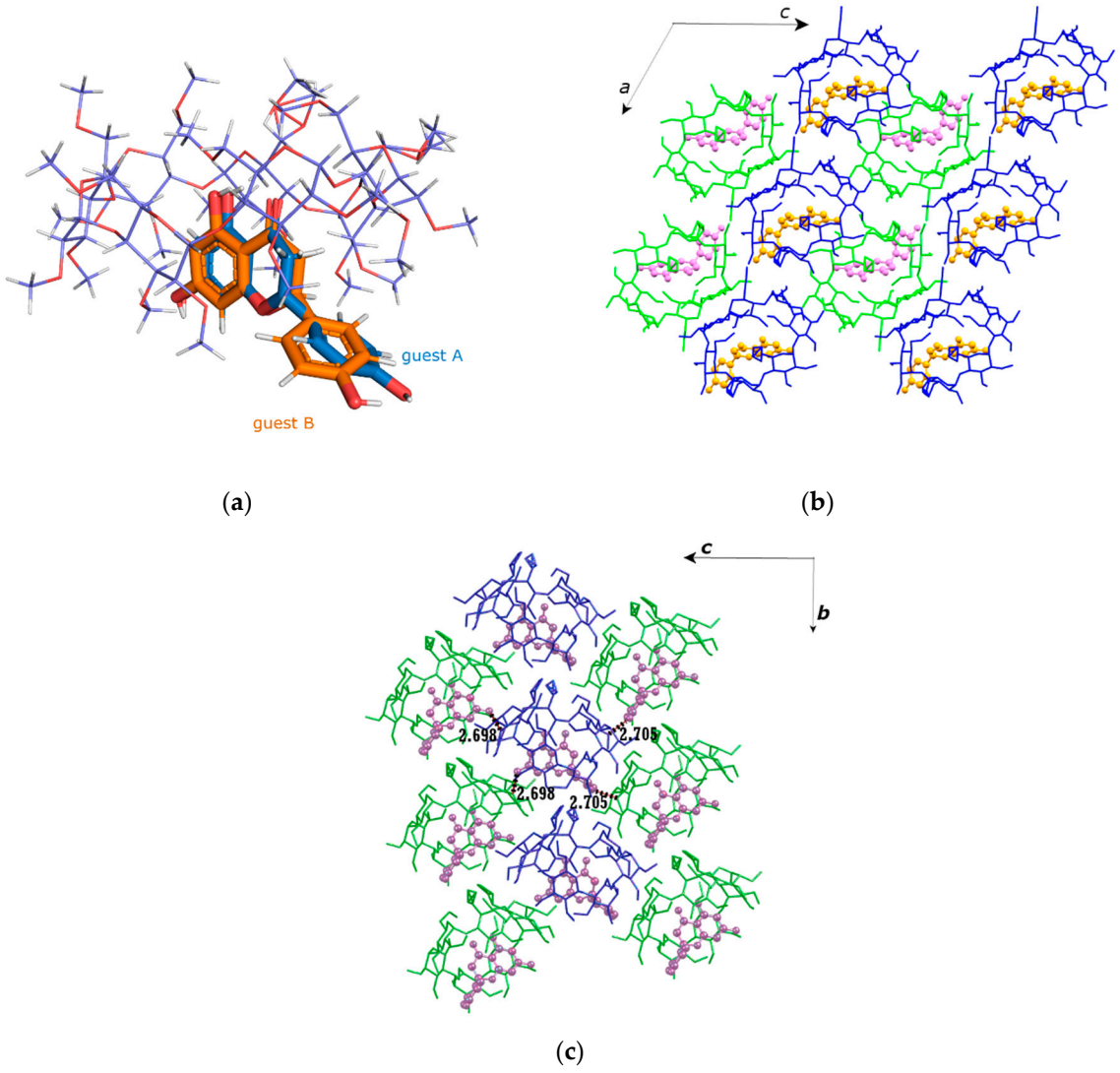

Figure 3. (**a**) The asymmetric unit of the naringenin/TM-*β*-CD inclusion complex; (**b**) projection onto the *ac* plane. The complex units of the columns deployed along the *a*-axis have opposite inclinations to the complex units of the columns deployed along the *c*-axis; and (**c**) projection onto the *bc* plane. Each complex unit is tightly packed in a cage-type mode with its open wide rim blocked by the primary and secondary methoxy groups of the adjacent complex units. Hydrogen bond distances (Å) between guest and host molecules of adjacent complex units are denoted.

2.2. Molecular Dynamics Studies

The structures of the 1:1 guest/host inclusion complexes of naringenin in DM-*β*-CD and TM-*β*-CD, as determined by x-ray crystallography, were subjected to NPT equilibration and subsequent molecular dynamics simulations at 300 K in explicit water solvent for 12 ns. The root mean square deviation

(RMSD) for the guest and the host molecules of both inclusion complexes as a function of MD simulations time is illustrated in Figure 4.

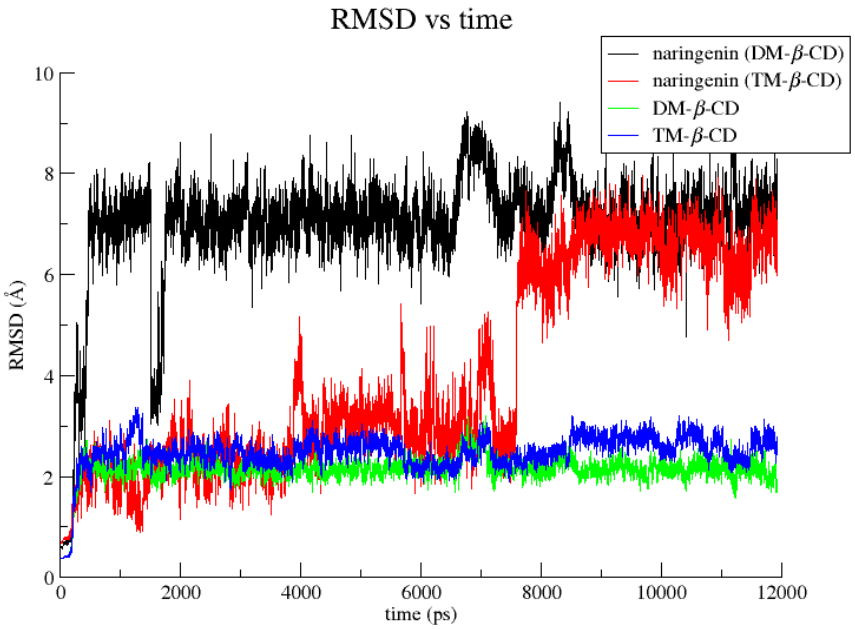

Figure 4. Root-mean-square deviation (RMSD) vs. time of guest and host molecules of naringenin/DM-*β*-CD and naringenin/TM-*β*-CD inclusion complexes.

In the case of naringenin/DM-*β*-CD, visual inspection of the simulation frames revealed that the guest molecule rapidly (in the first nanosecond) penetrates the primary rim of the host and is accommodated in a new position with its chromone group encapsulated axially in the hydrophobic cavity of the DM-*β*-CD and its 4-hydroxyphenyl residue (ring B) protruding extensively from the secondary rim of the host, exposed to the solvent (Figure 5a). This inclusion mode is retained during the time frame of the simulation. It has to be noted that, in the aqueous environment, the host did not maintain its rigid open-cone shape because its intramolecular interglucose hydrogen bonds net, which is observed in the crystalline state, is disrupted by hydrogen bonds formed between the secondary hydroxyl or methoxy groups of DM-*β*-CD and the ambient water molecules. This results in the distortion of the host macrocycle and the formation (in some time intervals, e.g., 6–7.5 ns and 8–8.5 ns) of a 'lid' by its primary methoxy groups (like in the case of the TM-*β*-CD host) that closes the primary narrow rim, enforcing the chromone of the guest molecule to move towards the wide rim of the host. In spite of the variation of its immersion depth in the cavity of the host, the entrapped chromone group never changes its axial orientation.

In contrast, in the case of the naringenin/TM-*β*-CD complex, the chromone group of the guest retains its crystallographically-determined equatorial accommodation in the wide rim of the host for about 7.5 ns. The characteristic 'lid' in the primary rim of TM-*β*-CD is maintained during the time frame of the simulation, restraining the chromone ring of the guest molecule to a shallow accommodation in the secondary rim of the host. However, the hydroxyls of ring A of the chromone are usually hydrogen-bonded with the secondary methoxy groups of the host molecule (Figure 6a), tethering the guest molecule to the host even when the chromone group of the guest molecule adopts an axial accommodation and its C ring protrudes from the wide rim of the host, as observed after 7 ns of simulation (Figure 5b).

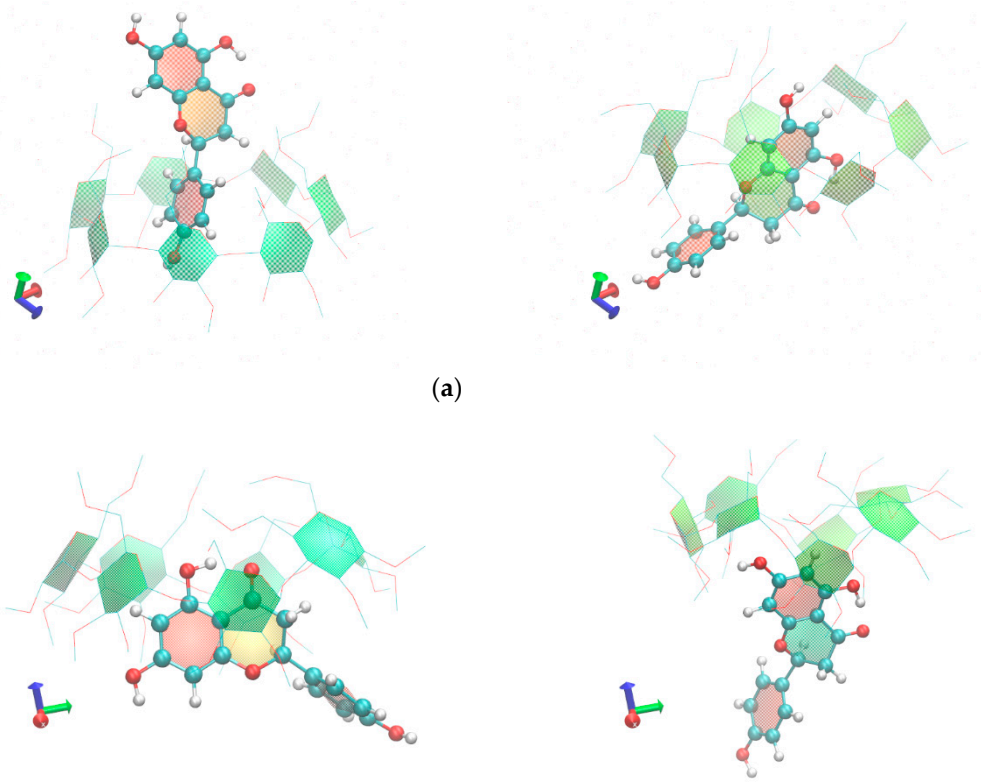

Figure 5. Representative snapshots for (**a**) naringenin/DM-β-CD at: 0 ns (left) and 2 ns (right), and for (**b**) naringenin/TM-β-CD at: 0 ns (left) and 8 ns (right). Guest molecules are depicted as ball-and-stick models and hosts' macrocycle as a paperchain.

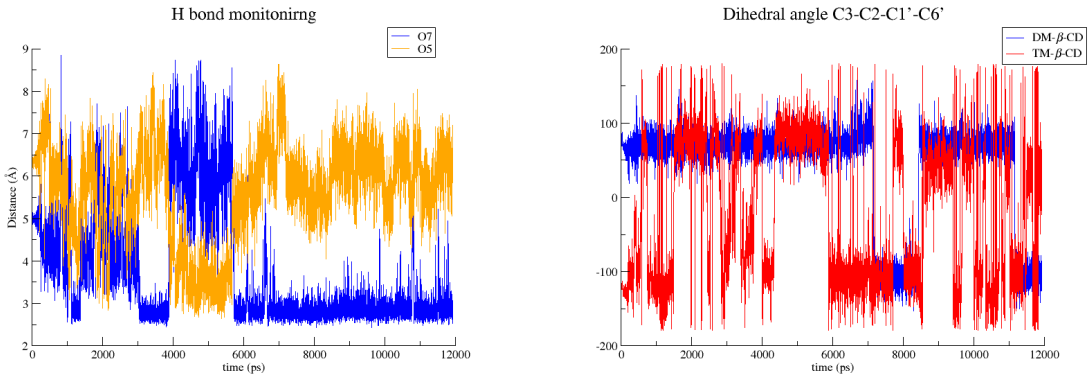

Figure 6. (**a**) H-bond monitoring between the hydroxyls of the ring A of the chromone group (atoms O7 and O5) of the guest molecule and the secondary methoxy group of the third glucose unit of TM-β-CD and (**b**) dihedral angle C3-C2-C1'-C6' of naringenin in both hosts.

Thus, by inspecting the MD simulation frames it is clear that naringenin is bound more tightly in the DM-β-CD than in the TM-β-CD cavity. The 4-hydroxyphenyl residue (ring B) of naringenin rotates about the C1'–C2 axis of the molecule much more frequently in the case of the TM-β-CD than the DM-β-CD host molecule, as indicated by the interchanges of the C3-C2-C1'-C6' dihedral angle of the guest molecule (Figure 6b).

These observations were also confirmed by the Molecular Mechanics/Generalized Born Surface Area (MM/GBSA) estimation of the binding affinities for both inclusion complexes (Table 1). From the values of the energetic components listed in Table 1, Van der Waals interactions are predominant in both cases. By comparing the binding affinities of both inclusion complexes and omitting the entropic term, it is clear that the calculated value $\Delta G_{(GB)}$ for naringenin/DM-β-CD is significantly higher than that of naringenin/TM-β-CD, indicating a more stable inclusion complex. A high $\Delta G_{(GB)}$ value for naringenin/DM-β-CD has also been estimated by Sangpheak et al. [18] although the calculation was based on a structure model (predicted by molecular docking) in which the orientation of the guest molecule was opposite to that of the crystal structure. Moreover, Yang et al. have reported binding affinity values estimated by spectral titration experiments for naringenin/DM-β-CD and naringenin/TM-β-CD inclusion complexes in a water/alcohol (v/v = 4:1) [14], which also indicate that naringenin/DM-β-CD is more stable than naringenin/TM-β-CD.

Table 1. Binding free energies (kcal/mole) of the naringenin inclusion complexes with the two methylated β-CDs calculated by MM/GBSA analysis.

Naringenin/*DM-β-CD*		**Naringenin/*TM-β-CD***
Enthalpic Term		
ΔE_{vdW}	−33.50 ± 2.77	−23.40 ± 4.63
ΔE_{ele}	−8.07 ± 2.46	−13.09 ± 3.25
ΔE_{GB}	21.95 ± 2.11	24.58 ± 3.24
ΔE_{surf}	−3.31 ± 0.16	−2.79 ± 0.29
ΔG_{gas}	−41.58 ± 3.9	−36.49 ± 6.02
ΔG_{solv}	18.64 ± 2.07	21.79 ± 3.18
[a] $\Delta G_{(GB)}$	−22.93 ± 2.75	−14.69 ± 3.94
Entropic Term		
$(T\Delta S)$	−18.19 ± 1.16	−17.69 ± 1.71
Binding Energy		
[b] (ΔG_{bind})	−4.74 ± 2.98	3.0 ± 4.29

ΔE_{vdW} = van der Waals contribution; ΔE_{ele} = electrostatic energy; ΔE_{GB} = Generalized Born (GB) calculation of the electrostatic contribution to the solvation free energy; ΔE_{surf} = nonpolar contribution to the solvation free energy; [a] $\Delta G_{(GB)} = \Delta G_{solv} + \Delta G_{gas;}$ [b] $\Delta G_{bind} = \Delta G_{(GB)} - (T\Delta S)$.

3. Materials and Methods

3.1. X-ray Crystallography

3.1.1. Sample Preparation

Naringenin (98% pure), DM-β-CD (with overmethylated homologs impurities), and TM-β-CD (≥98% pure) as white powders were purchased from Sigma-Aldrich and used as received. The crystalline inclusion complexes naringenin/DM-β-CD and naringenin/TM-β-CD were prepared by adding isomolar amounts of host (44.00 mg or 0.033 mmol of DM-β-CD; 44.17 mg or 0.033 mmol of TM-β-CD) and guest molecule (9 mg or 0.033 mmol of naringenin) in 2 mL of distilled water. The two final mixtures were stirred vigorously at room temperature for 45 min and subsequently maintained at 321 K for a period of 2 weeks. Rod-shaped and prismatic crystals suitable for X-ray diffraction measurements were produced in the case of naringenin/DM-β-CD and naringenin/TM-β-CD, respectively.

3.1.2. Data Collection and Reduction

The crystals were transferred from their mother liquor to a drop of cryoprotectant (paraffin oil) and picked up with a cryo-loop. They were subsequently exposed to a stream of evaporating N_2 at 100 (2) K. Data were collected on a Bruker D8-VENTURE diffractometer with Cu Kα radiation (λ = 1.54178 Å) and an Oxford Cryosystems low-temperature device. The Bruker SAINT Software

package [24] was used for the integration of the collected diffraction images and the multi-scan method for data absorption correction was applied with the program SADABS [25].

3.1.3. Crystal Structure Determination

The structure of the naringenin/DM-β-CD inclusion complex was solved by molecular replacement, using the atomic coordinates of the DM-β-CD macrocycle of the bithiophene/DM-β-CD complex [26]. The molecular replacement solution was obtained by a Patterson vector search and Fourier recycling using the DIRDIF99 package [27]. On the other hand, the structure of naringenin/TM-β-CD inclusion complex was solved by Patterson-seeded dual-space recycling with the SHELXD program [28]. Both structures were refined by full-matrix least squares against F^2 using SHELXL-2014/7 [29] through the SHELXLE GUI [30]. Soft restraints on bond lengths and angles were applied mainly to model the disordered guest molecule. The topology of the naringenin was obtained by the PRODRG2 webserver [31]. H-atoms of the host and guest molecules were positioned geometrically and refined using the riding model with Uiso values 1.2–1.5-times those of their parent atoms.

3.1.4. Crystallographic Analysis and Coordinates Deposition

The geometric analysis and illustration of the crystal structures was made using Mercury [32] and Olex2 [33] programs. Details of the crystallographic experiments and structures refinement are listed in Table 2. Full crystallographic information files can be obtained from the Cambridge Structural Database under the reference numbers of the Cambridge Crystallographic Data Centre (CCDC) 1959194 and 1959196.

Table 2. Experimental details and refinement statistics.

Crystal Data	**Naringenin/DM-β-CD**	**Naringenin/TM-β-CD**
Chemical formula	$C_{56}H_{98}O_{35}{\cdot}C_{15}H_{12}O_5{\cdot}4.6(H_2O)$	$C_{63}H_{112}O_{35}{\cdot}C_{15}H_{12}O_5$
M_r	1687	1701.76
Crystal system, space group	Orthorhombic, $P2_12_12_1$	Monoclinic, $P2_1$
Temperature (K)	100(2)	100(2)
Unit cell parameters a, b, c (Å)	15.531(1), 17.810(1), 30.149(2)	15.758(3), 12.913(2), 22.273(3) β = 109.936 (1) (°)
V (Å^3)	8340.1 (10)	4260.6 (13)
Z	4	2
Radiation type	Cu $K\alpha$	Cu $K\alpha$
μ (mm^{-1})	0.96	0.90
Crystal size (mm^3)	0.5 × 0.1 × 0.1	0.45 × 0.3 × 0.2
Data collection		
Diffractometer	Bruker *APEX*-II	Bruker *APEX*-II
Absorption correction	Multi-scan *SADABS2014*/5—Bruker AXS area detector scaling and absorption correction	Multi-scan *SADABS2014*/5 - Bruker AXS area detector scaling and absorption correction
T_{min}, T_{max}	0.583, 0.752	0.496, 0.753
No. of measured, independent, and observed [$I > 2\sigma(I)$] reflections	65,321, 11,718, 10,457	65,916, 15,008, 14,866
R_{int}	0.056	0.046
(sin θ/λ)$_{max}$ (Å^{-1})	0.556	0.596
Refinement		
$R[F^2 > 2\sigma(F^2)]$, $wR(F^2)$, S	0.056, 0.127, 1.05	0.043, 0.110, 1.06
No. of reflections	11,718	15,008
No. of parameters	959	1050
No. of restraints	80	147
H-atom treatment	H-atom parameters constrained	H-atom parameters constrained
$\Delta\rho_{max}$, $\Delta\rho_{min}$ (e Å^{-3})	0.51, −0.43	0.38, −0.35
Absolute structure	Flack x determined using 4169 quotients [(I+) − (I−)]/[(I+) + (I−)] (Parsons, Flack and Wagner, Acta Cryst. B69 (2013) 249–259).	Flack x determined using 6895 quotients [(I+) − (I−)]/[(I+) + (I−)] (Parsons, Flack and Wagner, Acta Cryst. B69 (2013) 249–259).
Absolute structure parameter	−0.04 (6)	0.07 (3)

3.2. Molecular Dynamics

The 3D models that were employed for molecular dynamics simulations are based on the high-resolution X-ray crystal structures of the naringenin/DM-β-CD and naringenin/TM-β-CD (1: 1 host/guest ratio) inclusion complexes from the present crystallographic analysis using the Amber12 software package [34]. Both DM-β-CD and TM-β-CD host molecules were prepared using the q4md-CD force field [35], which is suitable to simulate these kind of modified carbohydrates. Partial atomic charges and geometrical and topological parameters for naringenin were assigned by the ANTECHAMBER program [36] using the general AMBER force field (GAFF) parameters and the AM1-BCC methodology. The xLEaP module implemented in Amber suite was used to add H atoms in both systems. Consecutively, a periodic, octahedral solvent box around the complexes with a spacing distance of 10 Å from the solute surface was created using the TIP3P model. Minimization and MD calculations were performed with SANDER. The particle mesh Ewald approach was used to treat long-range electrostatic interactions, while the non-bonded cutoff distance was set to 10 Å. All covalent bonds involving hydrogen atoms were treated by the constraint algorithm SHAKE [37]. The periodic boundary condition with NPT ensemble (1 atm, 300 K) was applied for both models using a time step of 1 fs for an additional 12 ns. The detailed simulation protocol has been analytically described in a previous work [20]. The MD trajectories were processed and analyzed using CPPTRAJ [38] and VMD [39].

The generalized Born and surface area continuum solvation (MM/GBSA) method [40,41] was applied to estimate the binding free energy of the given inclusion complexes. The binding free energy $\Delta G_{(GB)}$ comprises the terms ΔG_{gas}, which is the summation of van der Waals and electrostatic interaction energies, and ΔG_{solv}, which is the summation of the polar solvation free energy calculated by a GB model and the nonpolar contribution to the solvation free energy based on the solvent-accessible surface area using Linear Combinations of Pairwise Overlaps (LCPO) method. Finally, the conformational entropy changes (ΔS) upon complexation were estimated from the normal mode approximation using the NMODE module, which is also implemented in the Amber 12 suite. The entropy term was calculated by extracting snapshots from the MD trajectory every 100 frames and added to the enthalpic term according to (1):

$$\Delta G_{bind} = \Delta G_{(GB)} - T\Delta S. \quad (1)$$

The entropy term is needed for the calculation of absolute affinities. However, as the calculation of a converged entropy value is often dubious [42], it is frequently neglected if only the relative binding free energy of similar inclusion complexes shall be analyzed. Herein, solely the $\Delta G_{(GB)}$ term was used for comparison between the binding affinities of the inclusion complexes of naringenin in DM-β-CD and TM-β-CD.

4. Conclusions

The crystal structure of the naringenin/DM-β-CD inclusion complex reveals an inclusion mode opposite to that previously predicted by molecular docking [18] and 2D-NMR (ROESY) spectrum analysis [14]. In particular, the guest molecule was inserting from the primary rim of the host with its 4-hydroxyphenyl residue (ring B) accommodated in the host cavity and its chromone group protruding from the narrow rim of the rigid, open-cone-shaped host. This accommodation is probably due to the crystal contacts as MD simulations in aqueous environment, based on the crystallographically-determined structure of the complex unit, show that the guest molecule rapidly penetrates the primary rim of the host, adopting a new position with its chromone group encapsulated axially in the hydrophobic cavity of the DM-β-CD and its 4-hydroxyphenyl residue protruding extensively from the secondary rim of the host. The guest naringenin retains this inclusion mode during the time frame of the simulation without changing its orientation. The role of the crystal contacts is also pronounced in the crystal packing of the naringenin/DM-β-CD complex units: DM-β-CD hosts

develop their self-inclusion tendency and adjacent complex units are packed in a 'herring bone' fashion, forming columns that are deployed parallel along the *b*-axis and antiparallel along the *c*-axis.

On the other hand, in the crystal structure of the naringenin/TM-*β*-CD inclusion complex, naringenin is found with its chromone group laying equatorially in the wide rim of the host and its 4-hydroxyphenyl residue protruding extensively from this wide rim. The TM-*β*-CD host adopts the conformation of a closed cone as its primary methoxy groups form the characteristic 'lid' in its narrow region. The severe distortion of the flexible TM-*β*-CD macrocycle pronounces the induced-fit mechanism of complexation. The complex units are tightly packed, anhydrous, in a cage-type mode with the open wide rim of the complex blocked by primary and secondary methoxy groups of the adjacent host molecules. MD simulations of the naringenin/TM-*β*-CD in an aqueous environment show that the chromone group of the guest molecule, accommodated shallowly in the wide rim of the host, can also adopt an axial orientation, always tethered to the secondary methoxy groups of the guest via hydrogen bonds.

MM/GBSA calculations of the binding affinities of both inclusion complexes resulted in a significantly higher $\Delta G_{(GB)}$ value for naringenin/DM-*β*-CD than naringenin/TM-*β*-CD, indicating a more stable inclusion complex in the case of naringenin in DM-*β*-CD. This result was also confirmed by previously reported binding affinity values, estimated by spectral titration experiments for these two inclusion complexes [14].

Supplementary Materials: The following are available online at http://www.mdpi.com/2073-4352/10/1/10/s1, Table S1: Naringenin/DM-*β*-CD inclusion complex: a1. Guest-host and guest-bridge water molecules interactions, a2. CH/π bonds between guest and host, a3. Hydrogen bonds between water molecules bridging adjacent complex units Naringenin/TM-*β*-CD inclusion complex: b1. Guest-host interactions b2. CH/π bonds between guest and host; Table S2: a1 Conformational characteristics of the host molecules of the Naringenin/DM-*β*-CD complex, a2. Conformational characteristics of the host molecules of the Naringenin/TM-*β*-CD complex, Video S1: MD simulation of Naringenin/DM-*β*-CD inclusion complex in water ambient; Video S2: MD simulation of Naringenin/TM-*β*-CD inclusion complex in water ambient.

Author Contributions: Conceptualization, K.B.; Methodology, A.P., E.C., and K.B.; Validation, A.P., E.C., and K.B.; Formal Analysis, A.P., E.C., and K.B.; Investigation, A.P., E.C., and K.B.; Writing-Original Draft Preparation, A.P., E.C., and K.B.; Writing-Review & Editing, A.P., E.C., and K.B.; Visualization, E.C. and K.B.; Supervision, K.B.; Project Administration, K.B.; Funding Acquisition, K.B. All authors have read and agreed to the published version of the manuscript.

Funding: This research received no external funding.

Acknowledgments: We acknowledge support of this work by the project "OPENSCREEN-GR: An Open-Access Research Infrastructure of Target-Based Screening Technologies and Chemical Biology for Human and Animal Health, Agriculture and Environment" (Grant MIS 5002691), which is implemented under the Action "Reinforcement of the Research and Innovation Infrastructure", funded by the Operational Programme "Competitiveness, Entrepreneurship and Innovation" (Grant NSRF 2014–2020) and co-financed by Greece and the European Union (European Regional Development Fund). We also acknowledge support of this work by the project "INSPIRED-The National Research Infrastructures on Integrated Structural Biology, Drug Screening Efforts and Drug Target Functional Characterization" (Grant MIS 5002550), which is implemented under the Action "Reinforcement of the Research and Innovation Infrastructure", funded by the Operational Programme "Competitiveness, Entrepreneurship and Innovation" (Grant NSRF 2014–2020) and co-financed by Greece and the European Union (European Regional Development Fund).

Conflicts of Interest: The authors declare no conflict of interest.

References

1. Rao, P.V.; Kiran, S.; Rohini, P.; Bhagyasree, P. Flavonoid: A review on Naringenin. *J. Pharmacogn. Phytochem.* **2017**, *6*, 2778–2783.
2. Patel, K.; Gadewar, M.; Tahilyani, V.; Patel, D.K. A review on pharmacological and analytical aspects of diosgenin: A concise report. *Nat. Prod. Bioprospecting* **2012**, *2*, 46–52. [CrossRef]
3. Zeng, W.; Jin, L.; Zhang, F.; Zhang, C.; Liang, W. Naringenin as a potential immunomodulator in therapeutics. *Pharmacol. Res.* **2018**, *135*, 122–126. [CrossRef] [PubMed]
4. Zaidun, N.H.; Thent, Z.C.; Latiff, A.A. Combating oxidative stress disorders with citrus flavonoid: Naringenin. *Life Sci.* **2018**, *208*, 111–122. [CrossRef] [PubMed]

5. Salehi, B.; Fokou, P.V.T.; Sharifi-Rad, M.; Zucca, P.; Pezzani, R.; Martins, N.; Sharifi-Rad, J. The Therapeutic Potential of Naringenin: A Review of Clinical Trials. *Pharmaceuticals* **2019**, *12*, 11. [CrossRef]
6. Karim, N.; Jia, Z.; Zheng, X.; Cui, S.; Chen, W. A recent review of citrus flavanone naringenin on metabolic diseases and its potential sources for high yield-production. *Trends Food Sci. Technol.* **2018**, *79*, 35–54. [CrossRef]
7. Sangpheak, W.; Kicuntod, J.; Schuster, R.; Rungrotmongkol, T.; Wolschann, P.; Kungwan, N.; Viernstein, H.; Mueller, M.; Pongsawasdi, P. Physical properties and biological activities of hesperetin and naringenin in complex with methylated β-cyclodextrin. *Beilstein J. Org. Chem.* **2015**, *11*, 2763–2773. [CrossRef]
8. Shulman, M.; Cohen, M.; Soto-Gutierrez, A.; Yagi, H.; Wang, H.; Goldwasser, J.; Lee-Parsons, C.W.; Benny-Ratsaby, O.; Yarmush, M.L.; Nahmias, Y. Enhancement of naringenin bioavailability by complexation with hydroxypropyl-beta-cyclodextrin. *PLoS ONE* **2011**, *6*, e18033. [CrossRef]
9. Valle, E.M.M.D. Cyclodextrins and their uses: A review. *Process. Biochem.* **2004**, *39*, 1033–1046. [CrossRef]
10. Astray, G.; Gonzalez-Barreiro, C.; Mejuto, J.C.; Rial-Otero, R.; Simal-Gándara, J. A review on the use of cyclodextrins in foods. *Food Hydrocoll.* **2009**, *23*, 1631–1640. [CrossRef]
11. Marques, H.M.C. A review on cyclodextrin encapsulation of essential oils and volatiles. *Flavour Fragr. J.* **2010**, *25*, 313–326. [CrossRef]
12. Suvarna, V.; Gujar, P.; Murahari, M. Complexation of phytochemicals with cyclodextrin derivatives - An insight. *Biomed. Pharmacother. Biomedecine Pharmacother.* **2017**, *88*, 1122–1144. [CrossRef] [PubMed]
13. Saokham, P.; Muankaew, C.; Jansook, P.; Loftsson, T. Solubility of Cyclodextrins and Drug/Cyclodextrin Complexes. *Molecules* **2018**, *23*, 1161. [CrossRef] [PubMed]
14. Yang, L.-J.; Ma, S.-X.; Zhou, S.-Y.; Chen, W.; Yuan, M.-W.; Yin, Y.-Q.; Yang, X.-D. Preparation and characterization of inclusion complexes of naringenin with beta-cyclodextrin or its derivative. *Carbohydr. Polym.* **2013**, *98*, 861–869. [CrossRef] [PubMed]
15. Xu, X.; Yu, H.; Hang, L.; Shao, Y.; Ding, S.; Yang, X. Preparation of naringenin/ beta-cyclodextrin complex and its more potent alleviative effect on choroidal neovascularization in rats. *BioMed Res. Int.* **2014**, *2014*, 623509. [CrossRef]
16. Semalty, A.; Tanwar, Y.S.; Semalty, M. Preparation and characterization of cyclodextrin inclusion complex of naringenin and critical comparison with phospholipid complexation for improving solubility and dissolution. *J. Therm. Anal. Calorim.* **2014**, *115*, 2471–2478. [CrossRef]
17. Wen, J.; Liu, B.; Yuan, E.; Ma, Y.; Zhu, Y. Preparation and physicochemical properties of the complex of naringenin with hydroxypropyl-beta-cyclodextrin. *Molecules* **2010**, *15*, 4401–4407. [CrossRef]
18. Sangpheak, W.; Khuntawee, W.; Wolschann, P.; Pongsawasdi, P.; Rungrotmongkol, T. Enhanced stability of a naringenin/2,6-dimethyl beta-cyclodextrin inclusion complex: Molecular dynamics and free energy calculations based on MM- and. *J. Mol. Graph. Model.* **2014**, *50*, 10–15. [CrossRef]
19. Aree, T.; Saenger, W.; Leibnitz, P.; Hoier, H. Crystal structure of heptakis(2,6-di-O-methyl)-β-cyclodextrin dihydrate: A water molecule in an apolar cavity. *Carbohydr. Res.* **1999**, *315*, 199–205. [CrossRef]
20. Bethanis, K.; Christoforides, E.; Tsorteki, F.; Fourtaka, K.; Mentzafos, D. Structural studies of the inclusion compounds of α-naphthaleneacetic acid in heptakis(2,6-di-O-methyl)-β-Cyclodextrin and heptakis(2,3,6-tri-O-methyl)-β-Cyclodextrin by X-ray crystallography and molecular dynamics. *J. Incl. Phenom. Macrocycl. Chem.* **2018**, *92*, 157–171. [CrossRef]
21. Fourtaka, K.; Christoforides, E.; Mentzafos, D.; Bethanis, K. Crystal structures and molecular dynamics studies of the inclusion compounds of β-citronellol in β-cyclodextrin, heptakis(2,6-di-O-methyl)-β-cyclodextrin and heptakis(2,3,6-tri-O-methyl)-β-cyclodextrin. *J. Mol. Struct.* **2018**, *1161*, 1–8. [CrossRef]
22. Steiner, T.; Saenger, W. Crystal structure of anhydrous heptakis-(2,6-di-O-methyl) cyclomaltoheptaose (dimethyl-β-cyclodextrin). *Carbohydr. Res.* **1995**, *275*, 73–82. [CrossRef]
23. Caira, M.R.; Griffith, V.J.; Nassimbeni, L.R.; Oudtshoorn, B.V. X-ray structures of 1:1 complexes of (L)-menthol with β-cyclodextrin and permethylated β-cyclodextrin. *Supramol. Chem.* **1996**, *7*, 119–124. [CrossRef]
24. *SAINT*; SAINT Version 8.34A; Bruker-AXS: Madison, WI, USA, 2013.
25. Sheldrick, G.M. *SADABS*; SADABS Version 2012/1, 1; Bruker-AXS: Madison, WI, USA, 2012.
26. Takashima, Y.; Sakamoto, K.; Oizumi, Y.; Yamaguchi, H.; Kamitori, S.; Harada, A. Complex Formation of Cyclodextrins with Various Thiophenes and their Polymerization in Water: Preparation of Poly-pseudo-rotaxanes containing Poly(thiophene)s. *J. Incl. Phenom. Macrocycl. Chem.* **2006**, *56*, 45–53. [CrossRef]

27. Beurskens, P.T.; Beurskens, G.; Gelder, R.d.; Garcia-Granda, S.; Gould, R.O.; Smits, J.M.M. *The DIRDIF2008 Program System*; Crystallography Laboratory, University of Nijmegen: Nijmegen, The Netherlands, 2008; Available online: http://www.xtal.science.ru.nl/dirdif/software/dirdif.html (accessed on 18 December 2019).
28. Sheldrick, G.M. Experimental phasing with *SHELXC/D/E*: Combining chain tracing with density modification. *Acta Crystallogr. Sect. D* **2010**, *66*, 479–485. [CrossRef] [PubMed]
29. Sheldrick, G.M. Crystal structure refinement with *SHELXL*. *Acta Crystallogr. Sect. C* **2015**, *71*, 3–8. [CrossRef]
30. Hübschle, C.B.; Sheldrick, G.M.; Dittrich, B. *ShelXle*: A Qt graphical user interface for *SHELXL*. *J. Appl. Crystallogr.* **2011**, *44*, 1281–1284. [CrossRef] [PubMed]
31. Schüttelkopf, A.W.; van Aalten, D.M.F. *PRODRG*: A tool for high-throughput crystallography of protein–ligand complexes. *Acta Crystallogr. D Biol. Crystallogr.* **2004**, *60*, 1355–1363. [CrossRef] [PubMed]
32. Macrae, C.F.; Bruno, I.J.; Chisholm, J.A.; Edgington, P.R.; McCabe, P.; Pidcock, E.; Rodriguez-Monge, L.; Taylor, R.; van de Streek, J.; Wood, P.A. *Mercury* CSD 2.0 – new features for the visualization and investigation of crystal structures. *J. Appl. Crystallogr.* **2008**, *41*, 466–470. [CrossRef]
33. Dolomanov, O.V.; Bourhis, L.J.; Gildea, R.J.; Howard, J.A.K.; Puschmann, H. OLEX2: A complete structure solution, refinement and analysis program. *J. Appl. Crystallogr.* **2009**, *42*, 339–341. [CrossRef]
34. Salomon-Ferrer, R.; Case, D.A.; Walker, R.C. An overview of the Amber biomolecular simulation package. *Wiley Interdiscip. Rev. Comput. Mol. Sci.* **2012**, *3*, 198–210. [CrossRef]
35. Cezard, C.; Trivelli, X.; Aubry, F.; Djedaini-Pilard, F.; Dupradeau, F.-Y. Molecular dynamics studies of native and substituted cyclodextrins in different media: 1. Charge derivation and force field performances. *Phys. Chem. Chem. Phys.* **2011**, *13*, 15103–15121. [CrossRef] [PubMed]
36. Wang, J.; Wang, W.; Kollman, P.A.; Case, D.A. Automatic atom type and bond type perception in molecular mechanical calculations. *J. Mol. Graph. Model.* **2006**, *25*, 247–260. [CrossRef] [PubMed]
37. Kräutler, V.; van Gunsteren, W.F.; Hünenberger, P.H. A fast SHAKE algorithm to solve distance constraint equations for small molecules in molecular dynamics simulations. *J. Comput. Chem.* **2001**, *22*, 501–508. [CrossRef]
38. Roe, D.R.; Cheatham, T.E., 3rd. PTRAJ and CPPTRAJ: Software for Processing and Analysis of Molecular Dynamics Trajectory Data. *J. Chem. Theory Comput.* **2013**, *9*, 3084–3095. [CrossRef] [PubMed]
39. Humphrey, W.; Dalke, A.; Schulten, K. VMD: Visual molecular dynamics. *J. Mol. Graph.* **1996**, *14*, 27–28, 33–38. [CrossRef]
40. Miller, B.R., 3rd; McGee, T.D.J.; Swails, J.M.; Homeyer, N.; Gohlke, H.; Roitberg, A.E. MMPBSA.py: An Efficient Program for End-State Free Energy Calculations. *J. Chem. Theory Comput.* **2012**, *8*, 3314–3321. [CrossRef]
41. Wang, J.; Morin, P.; Wang, W.; Kollman, P.A. Use of MM-PBSA in Reproducing the Binding Free Energies to HIV-1 RT of TIBO Derivatives and Predicting the Binding Mode to HIV-1 RT of Efavirenz by Docking and MM-PBSA. *J. Am. Chem. Soc.* **2001**, *123*, 5221–5230. [CrossRef] [PubMed]
42. Genheden, S.; Ryde, U. The MM/PBSA and MM/GBSA methods to estimate ligand-binding affinities. *Expert Opin. Drug Discov.* **2015**, *10*, 449–461. [CrossRef] [PubMed]